HHS Public Access

Author manuscript

IEEE Trans Biomed Eng. Author manuscript; available in PMC 2024 August 01.

Published in final edited form as:

IEEE Trans Biomed Eng. 2023 August ; 70(8): 2279–2288. doi:10.1109/TBME.2023.3240725.

Miniaturized Stacked Transducer for Intravascular Sonothrombolysis with Internal-illumination Photoacoustic Imaging Guidance and Clot Characterization

Huaiyu Wu,
Department of Mechanical & Aerospace Engineering, North Carolina State University, Raleigh, NC 27695 USA.

Yuqi Tang,
Department of Biomedical Engineering, Duke University, Durham, NC 27708, USA.

Bohua Zhang,
Department of Mechanical & Aerospace Engineering, North Carolina State University, Raleigh, NC 27695 USA.

Paul Klippel,
Graduate Program in Acoustics and Department of Biomedical Engineering, Pennsylvania State University, University Park, PA 16802, USA.

Yun Jing,
Graduate Program in Acoustics and Department of Biomedical Engineering, Pennsylvania State University, University Park, PA 16802, USA.

Junjie Yao,
Department of Biomedical Engineering, Duke University, Durham, NC 27708, USA.

Xiaoning Jiang
Department of Mechanical & Aerospace Engineering, North Carolina State University, Raleigh, NC 27695 USA.

Abstract

Thromboembolism in blood vessels can lead to stroke or heart attack and even sudden death unless brought under control. Sonothrombolysis enhanced by ultrasound contrast agents has shown promising outcome on effective treatment of thromboembolism. Intravascular sonothrombolysis was also reported recently with a potential for effective and safe treatment of deep thrombosis. Despite the promising treatment results, the treatment efficiency for clinical application may not be optimized due to the lack of imaging guidance and clot characterization during the thrombolysis procedure. In this paper, a miniaturized transducer was designed to have an 8-layer PZT-5A stacked with an aperture size of 1.4 ×1.4 mm^2 and assembled in a customized two-

Corresponding authors': junjie.yao@duke.edu, xjiang5@ncsu.
Huaiyu Wu and Yuqi Tang contributed equally to this work.

CONFLICT OF INTEREST

Xiaoning Jiang has a financial interest in SonoVascular, Inc., which licensed an intravascular sonothrombolysis technology from NC State.

lumen 10-Fr catheter for intravascular sonothrombolysis. The treatment process was monitored with internal-illumination photoacoustic tomography (II-PAT), a hybrid imaging modality that combines the rich contrast of optical absorption and the deep penetration of ultrasound detection. With intravascular light delivery using a thin optical fiber integrated with the intravascular catheter, II-PAT overcomes the penetration depth limited by strong optical attenuation of tissue. *In-vitro* PAT-guided sonothrombolysis experiments were carried out with synthetic blood clots embedded in tissue phantom. Clot position, shape, stiffness, and oxygenation level can be estimated by II-PAT at clinically relevant depth of ten centimeters. Our findings have demonstrated the feasibility of the proposed PAT-guided intravascular sonothrombolysis with real-time feedback during the treatment process.

Index Terms—

Intravascular ultrasound transducer; Sonothrombolysis; Deep tissue imaging; Functional imaging; Photoacoustic imaging; Internal illumination

I. INTRODUCTION

With high morbidity and mortality, the venous thromboembolism (VTE) is one of the leading causes of death worldwide. The deep vein thrombosis (DVT), which usually starts in calf veins, may extend to proximal veins and subsequently break free to cause pulmonary embolism (PE) if the debris enters the lungs. [1]-[3] Annually, 10% of symptomatic PE cases result in death within 1 hour of onset and as many as 300,000 people in the United States die from acute pulmonary embolism [1], [4]. However, the treatment of the VTE is difficult and costly. Approximately 50% of patients with symptomatic proximal DVT or PE have recurrent thrombosis within three months after treatment. Traditionally, VTE has been treated with systemic thrombolysis using tissue plasminogen activator (tPA) or the mechanical thrombectomy [5]-[8]. However, the former method has the drawbacks of long treatment time (over 24 hours) and high risk of symptomatic hemorrhage [5], [9], while the latter carries risk of vascular damage and has limited clinical improvement compared with t-PA alone [7], [8], [10].

For thrombolysis therapeutic application, techniques are required to either locally increase the efficacy of thrombolytic drugs, or allow minimally invasive mechanical treatment of the thrombus without drugs. Ultrasound enhanced thrombolysis, or sonothrombolysis, was reported to have the potential for both [11], [12]. Research has shown that pulsed ultrasound increased the thrombolytic efficacy *in-vitro* compared to continuous wave ultrasound. By generating stable and inertial cavitations, the histotripsy pulses were reported to be efficient in dissolving clots with stiff and dense bio-structures [13], [14]. Additionally, with the ultrasound contrast agents (UCAs) including microbubbles (MBs) and nanodroplets (NDs), sonothrombolysis has shown advantages in treating both non-retracted and retracted clots by reducing the threshold for inducing cavitation [15]-[19]. Subsequent studies indicated there was thrombolytic enhancement using either sub-megahertz ultrasound exposure or the diagnostic imaging frequencies [20], [21]. Yet, treatment with external transducers or arrays also were limited due to the significant attenuation and aberration from the

biological tissues, such as frequency-dependent attenuation by the soft tissues and blockage by the bones [20]-[24]. Respiratory motion can result in poor acoustic coupling at the skin-transducer interface, and subsequently skin-burn or vessel damage. The relatively large size difference between the focal zone and the blood vessels can potentially result in moderate collateral damage *in-vivo* in forms of coagulative necrosis or hemorrhage. [25]-[27].

More recently, a miniaturized intravascular transducer has been proposed to provide a high efficiency for *in-vitro* sonothrombolysis [15]. By delivering the UCAs locally to the clot, a relatively low peak-negative pressure and a small focal zone are needed for the MB/ND-mediated sonothrombolysis. The preliminary *ex-vivo* test results indicated no vessel wall damage during the treatment [28]. Yet, thrombolysis treatment is usually accompanied by anticoagulation therapy. Depending on the clot characteristics, anticoagulation drugs make the vessels more vulnerable and thus the thrombolysis faces the challenges of either VTE recurrence or bleeding [29]-[32]. To minimize the risk and potential post-treatment complications, a diagnostic imaging method is needed to guide therapy with the capability of characterizing the clot structure and composition [32].

Both non-invasive and invasive ultrasound approaches have been used for blood clot detections *in vitro* and *in vivo*. Quantitative ultrasound parameters were used under static or dynamic conditions, including backscattering, attenuation and sound velocity [32]-[34]. For non-invasive clot detection, B-mode and Doppler ultrasound imaging are commonly applied in the clinical applications [35]-[38]. For clot characterization, ultrasound shear-wave-based approach was applied *in-vitro* and strain imaging was used *in vivo* [39], [40]. For invasive clot detection, a high-frequency needle transducer was used for measuring elastic tissue property. Invasive shear wave imaging was also realized with the dual-element needle transducer [41]. For deep vein clot detection, however, B-mode US imaging may have low sensitivity and resolution, while Doppler US imaging relies on existing blood flow and cannot detect fully occluded vessels [42]. Most of the shear wave elastography (SWE) approaches may be affected by the tissue inhomogeneity. The wave transmission and reflection in SWE may interfere with different boundary conditions, and thus lead to inaccurate measurement [43], [44]. By contrast, photoacoustic tomography (PAT) combines the rich contrast of optical absorption and the deep penetration of ultrasound waves. Hemoglobin, one of the major components of clots, is one of the most used endogenous contrasts in PAT. Therefore, hemoglobin can be readily imaged by PAT to provide both structural and functional information of the clots [45]. Our previous study has also shown that the retractiveness and the age of the clot can be estimated from the acoustic frequency spectrum of the PA signal and the oxygen saturation of the clot hemoglobin [46]. Conventional PAT uses external light illumination, yet deep veins are typically several centimeters beneath the skin surface. Thus, the imaging depth of conventional PAT with external light illumination is limited due to strong light attenuation of the tissue and the accuracy of the functional quantification such as oxygenation measurement is severely compromised without optical fluence compensation. To overcome these issues, we have developed a new illumination strategy by delivering the light through a thin optical fiber inside the organ cavity such as the ureter, a technology referred to as internal-illumination photoacoustic tomography (II-PAT), which has demonstrated an imaging depth of >10 cm in biological tissues [47].

In this work, we developed a miniaturized sub-megahertz (500 kHz) transducer coupled with a UCA injection tube for the microbubble-mediated sonothrombolysis. The treatment process was monitored by II-PAT with intravascular light delivery using a thin optical fiber to overcome the limited imaging depth. The position, stiffness, and oxygenation level of the clots were estimated beneath ten-centimeter-thick tissue. The findings suggested the proposed PAT guided intravascular sonothrombolysis is highly promising in simultaneous clot detection, characterization, and treatment.

II. MATERIALS AND METHODS

A. Stacked transducer design and fabrication

With a small aperture size, a single layer transducer has a relatively large electrical impedance and less efficient pressure output. Therefore, we adopted an 8-layer stacked design to increase the capacitance and lower the electrical impedance for better electrical impedance matching with the driving electronics, which consequently increased the pressure output under the same driving conditions. The piezoelectric stacked transducers were designed and fabricated with a similar method as reported in [15]. PZT-5A (Type III 301, TRS Technologies, Inc., State College, PA, US) was chosen as the active layers due to its relatively high piezoelectric coefficient. The mixed Al_2O_3/epoxy (weight ratio = 1:4) was applied as the isolation layer from the side of the transducer. As shown in Fig. 1 eight layers of PZT-5A were stacked with the thickness of 250 μm each. The designed center frequency of the stack transducer was 500 kHz. Between every two layers, conductive silver epoxy (E-Solder 3022, Von-Roll Inc., Cleveland, OH, US) was used for bonding. By maintaining the pressing pressure with a customized jig, the thickness of the bonding layer was controlled to 25 μm. Then, the 50 nm Al_2O_3 particles were mixed with epoxy (EPO-TEK 301, Epoxy tech. Inc., Billerica, MA, US) with a volume ratio of 25% to obtain a relatively high acoustic impedance matching. The matching layer made of Al_2O_3/epoxy was lapped to 1 mm for the designed frequency of 500 kHz. Then the stacks were diced into a dimension of 1.4 mm × 1.4 mm, which was small enough for intravascular use (10-French catheter). Then, an Al_2O_3/epoxy layer was attached to the side of the transducer as an insulation layer, which was moldable before curing process with a relatively large electrical resistance. After that, the side electrodes were connected with silver epoxy with an electric resistance less than 1 Ω. After wire connection, a 13-μm-thick parylene layer was coated on the whole transducer as the passivation layer. The working frequency and pressure output of the transducer was simulated and estimated using a symmetrical model in COMSOL (COMSOL 5.5, COMSOL Inc. Burlington, MA, US). Table I shows the main design parameters for each layer in the stacked transducer. Then, the transducer was assembled into the 10-Fr catheter and fixed with epoxy (EPO-TEK 301, Epoxy tech. Inc., Billerica, MA, US). A multimode fiber (FT1500UMT, Thorlabs, Newton, NJ, US) with a numerical aperture of 0.39 mm and core diameter of 1.5 mm was bonded to the catheter for laser light delivery for II-PAT.

B. Stacked transducer characterization

The prototyped transducer was characterized for its electric impedance response and acoustic pressure output. To measure the electric impedance, the transducer was connected to an impedance analyzer (4294A, Agilent Tech. Inc., Santa Clara, CA, US). and the

response was measured in the frequency range from 0.2 to 1.0 MHz. To confirm the integrity of the fabricated transducer, the impedance curve was compared with the simulation result using the COMSOL model. To measure the pressure output by the transducer, a function generator (33250A, Agilent Tech. Inc., Santa Clara, CA, US) was first connected to the power amplifier with a power gain of 28 dB (75A250A, AR, Souderton, PA, US). Then the transducer was excited with a sinusoidal pulse of 10 cycles per 10 ms in a water tank. A hydrophone (HGL-0085, ONDA Crop. Sunnyvale, CA, US) and a 20 dB preamplifier (AH-2020, ONDA Crop. Sunnyvale, CA, US) were used to detect the acoustic pressure output of the stacked transducer. The pressure outputs under different input driving voltages were measured.

C. Blood Clot Preparation

To prepare the blood clot, a Polydimethylsiloxane (PDMS) channel was first prepared to mimic the deep vein. As shown in Fig. 2, a customized mold was used to form a main channel with a diameter of 7 mm for positioning the clot and a side channel with a diameter of 2 mm as the outlet of the clot debris. Then, the blood clot samples were prepared following the method in our previous work [15]. The acid citrate dextrose (ACD) bovine blood (Lampire Biological Lab Inc., Pipersville, PA, US) was added with the 2.75% W/V calcium chloride solution (Fisher Scientific, Fair Lawn, NJ, US) with a volume ratio of 10:1. The mixture was drained into the PDMS channel and sealed. The containers were immersed in 37 °C water bath for 3 hours. After that, all the samples were stored at 4 °C for 3 days to achieve full incubation. In each test, the sample was made with a length of 10 mm.

D. In-vitro sonothrombolysis tests and PAT

The two openings of the PDMS channel were connected to the PBS-filled Tygon tubes (4.76 mm inner diameter) and immersed in water. To demonstrate the deep tissue imaging capability, around 10-cm chicken breast tissue was placed between the photoacoustic imaging transducer array and the PDMS channel. During the thrombolysis tests, a burst signal at 485 kHz was generated with the function generator at a pulse repetition rate of 200 Hz. Each burst contained 125 cycles, corresponding to a duty cycle of 5%. The input voltage was 90 V_{pp}, and peak-negative pressure output was ~2.8 MPa. The microbubbles used in the previous work were injected as the cavitation agents with a concentration of 10^9/mL at a flow rate of 100 μL/min [48], [49]. After every 10 min treatment, the treatment catheter was advanced by 1 mm towards the clot in order to maintain the distance between the transducer and the receding clot.

A linear array transducer (L7–4, Philips ATL, Atlanta, GA, US) with 128 elements, a central frequency of 5 MHz, and a −6 dB receiving bandwidth of 85% was connected to a commercial ultrasound scanner (Vantage 256, Verasonics, Kirkland, WA, US) for PA data acquisition. Laser pulses at 700 and 800 nm were coupled into the multimode fiber for internal illumination with a pulse energy of 11 mJ per wavelength at the output of the fiber. The optical fluence on the clot surface at both wavelengths was ~8.8 mJ/cm^2, which was within the ANSI limit [50], [51]. The distal end of the fiber was around 5 mm from the clot surface. After each treatment session, 300 frames of two-dimensional PA images were acquired at each wavelength. Delay-and-sum (DAS) and delay-multiply-and-

sum (DMAS) algorithms were used for image reconstruction [52],[53]. To estimate the oxygenation saturation of hemoglobin (sO_2) of the clot, DAS was used as it preserved the linear dependenc e of PA signal on the optical absorption. However, the DAS results had strong limited-view artifacts [54],[55], and thus DMAS, which is a non-linear process and superior in artifact suppression, was used to mask out the limited-view artifacts in the DAS images. The sO_2 map of the clot was estimated using the linear spectral unmixing method on the masked DAS images after 300-frame-averaging. The raw PA channel signals acquired at 800 nm were used to obtain the acoustic frequency spectra of the clots.

To demonstrate the improved treatment outcomes from sonothrombolysis with microbubbles, three treatment conditions were applied to the same batch of clots: 1) sonothrombolysis with microbubble infusion (US+MB), 2) sonothrombolysis alone (US), 3) microbubble infusion alone (MB). For each treatment condition, four 10-minute treatment sessions were applied, and the clots were imaged and characterized by II-PAT after each treatment session.

E. Passive cavitation detection

Passive cavitation detection (PCD) was performed in order to examine the cavitation activities in sonothrombolysis. To generate cavitation, a function generator (33250A, Agilent Tech. Inc., Santa Clara, CA, US) was first connected to the power amplifier with a power gain of 28 dB (75A250A, AR, Souderton, PA, US). Then the stacked transducer was excited with a sinusoidal pulse of 25 cycles per 1 ms in a water tank under 90 V_{pp}. The cavitation acoustic signals were received with a hydrophone (HGL-0085, ONDA Corp., Sunnyvale, CA) and recorded with an oscilloscope (DSO7104B, Agilent Technologies, Santa Clara, CA, US). Three groups of signals were collected and analyzed with 16-time averaging. The inertial and stable cavitation doses were then calculated using the averaged amplitude of the spectrum using MATLAB (MATLAB R2018b, Mathworks, Natick, MA, US). The stable cavitation dose was from the 2nd harmonic signal. A 5th order Butterworth bandpass filter was applied at the 2nd harmonic frequency ($2f_0 \pm 0.5f_0$) [16]. After filtering, the signals were transformed into the frequency domain. The area under the curve (AUC) of the 2nd harmonic ($1.5\ f_0 - 2.5f_0$) in the frequency spectrum was calculated and the averaged results from three repeated data sets were used as the stable cavitation dose. To calculate the inertial cavitation dose, a similar method was applied with a bandpass filter around the 3rd to the 6th harmonic frequency. The AUC in the frequency range of 1.5 – 3.5 MHz was calculated and the selective AUCs at harmonic frequencies were subtracted ($3f_0$, $4f_0$, $5f_0$, $6f_0$, $\pm$ 0.2 f_0 MHz) with those from the stable cavitation.

III. RESULTS

A. Stacked treatment transducer characterization.

Fig. 3 shows the simulation and measured results of the designed treatment transducer. As shown in Fig. 3(a), the simulated resonant frequency was 500 kHz with an electrical impedance of 215 Ω. Under 90 Vpp input voltage, the simulated peak-to-peak (PTP) pressure was 4.8 MPa in Fig. 3(c). Based on the simulation results, we fabricated the stacked transducer and characterized the performance of the transducer in terms of electric

impedance and acoustic pressure output. Fig. 3(b) represents the electric impedance of the fabricated device. The impedance was about 253 Ohm at 486 kHz, showing a high agreement (~2.8% discrepancy) with the simulation result in Fig. 3(a). The difference of the impedance between the measurement and the simulation could be caused by acoustic property differences of the materials between the simulation and the actual fabricated device. Fig. 3(b) shows the measured acoustic pressure output. The sensitivity of the transducer was 0.059 MPa/V_{pp}, which gives a peak-to-peak pressure (PTP) of 4.7 MPa and a peak-negative pressure (PNP) of 2.3 MPa when driven at 90 V_{pp}, respectively. The high PNP level was able to induce cavitation from the microbubbles [56].

B. II-PAT characterization of the blood clots.

The reconstructed PA images and sO_2 estimation can provide the general morphological and functional information of the clots, as previously reported [46]. Fig. 4 shows the estimated sO_2 and morphological change of the clots under three different treatment conditions. Since the bovine blood was well-mixed with the $CaCl_2$ solution before clotting, and no further gas exchange was expected during the clot formation or the treatment process, the sO_2 was expected to remain relatively homogeneous inside the clots. However, discoloration was observed during the treatment process for all treatment conditions, potentially due to the immersion of clots in PBS and the loosening clot structure. The gradual change in hemoglobin concentration can lead to color change during the treatment process. The clot front surface facing the treatment transducer was localized at t = 0 min and 40 min. As the clot was effectively stationary during the treatment process, the changes in the clot front surface were used for estimating the change in total clot length. A significant clot length reduction of 5.1 mm by sonothrombolysis with microbubbles (US+MB) was observed (Fig. 4a). Meanwhile, the ultrasound-only treatment (US) resulted in a moderate decrease of 1.9 mm in clot length (Fig. 4b), and no difference before and after the treatment was observed with microbubble only treatment (MB) (Fig. 4c). The results indicated remarkable improvement in lysis efficiency achieved by sonothrombolysis with microbubbles.

The acoustic frequency spectra of PA signals at 800 nm also reflect the stiffness change of the clot under each treatment condition in Fig. 5. As demonstrated in our previous study [46], retracted clots with stiff structures and densely packed red blood cells generate more low frequency PA signals, while unretracted clots generate more high frequency PA signals. After 40-min treatment, the frequency spectra showed different shift patterns for each treatment condition. For MB only treatment condition, MBs may still remain attached to the clot surface after flushing with PBS, and thus attenuate the light intensity delivered to the clot. The spectra from the MB-only treatment showed little change in the frequency components, despite the slight increase in the high frequency components, likely due to the presence of microbubbles and attenuated optical fluence delivered to the clot (Fig. 5c). With ultrasound-only treatment, a reduction in the low frequency components was observed Fig. 5b). The reduction in low frequency components was related to loosening of the clot structure, as ultrasound alone can induce mechanical disruption and streaming effect, which can cause disaggregation of large fibrin bundles into small bundles. When microbubbles were infused in addition to the ultrasound treatment, the high frequency components increased due to clot dissolution and thus reduced red blood cell packing

density, and yet the low frequency component also significantly increased in the spectrum, which indicated an increase in stiffness of the remaining clot (Fig. 5a). The increase in clot stiffness was also observed and demonstrated by Auboire et al [57]-[59].

The clot size reduction with the cross-section view under the three treatment conditions is shown in Fig. 7. For the sonothrombolysis with microbubble infusion, the clot showed the most dissolution in size with a total flow recovery. The tunnel had an estimated diameter of 3.1 mm, which was almost twice of the aperture size of the stacked transducer. As a comparison, Fig. 7(b) shows the clot size reduction with US-only treatment and dissolution of the clot on the surface was observed with a diameter less than 2 mm, which was close to the transducer aperture size and thus indicated a mechanical drilling effect during the feeding process of the catheter in a limited area. The improvement in the lysis efficiency indicated a positive effect of microbubble cavitations. Fig. 7(c) showed no significant changes in the clot size induced by the microbubble-only treatment. The clot showed a slight unevenness on the surface which was likely due to the sample preparation.

C. Passive Cavitation Detection

Fig. 6 shows the enhancement of cavitation with US+MB treatment compared with US-only treatment. For the stable cavitation, the averaged bandpass filtered (0.75–1.25 MHz) signals were acquired, shown in Fig. 6(a). The results showed a significant enhancement of the second harmonics and ultra-harmonics by the US+MB treatment compared with the US-only treatment. Meanwhile, the US-only data showed weak second harmonic signals ($2f_0$) after filtering, which was due to the relatively strong input peak-negative pressure and the nonlinear interactions of the ultrasound waves with the clot and the PDMS channel [60], [61]. To estimate the cavitation dose difference between the US+MB and US-only treatment condition, the area under the curve (AUC) of the spectrum was calculated. As shown in Fig. 6(c), the US+MB group had a cavitation dose of 0.26 V Hz over that 0.03 V·Hz of the US-only group, reflecting 8-fold enhancement in the stable cavitation by the microbubbles.

Then we analyzed the inertial cavitation level with each treatment condition using bandpass filtered (1.25 – 3.25 MHz) signals, which were generated by cavitation-induced shock waves. As shown in Fig. 6(b), the US+MB group had stronger broad band shockwave signals compared with the US-only group, reflecting the inertial cavitation enhancement. When estimating the inertial cavitation, the content around the super harmonics were removed at higher frequencies ($3f_0$, $4f_0$, $5f_0$, $6f_0$ ±0.1 MHz) to minimize the contribution by stable cavitation. Fig. 6(c) shows the inertial cavitation dose of 2.68 V·Hz for US+MB and 0.52 V·Hz for US-only, reflecting a 5-fold enhancement due to microbubbles.

IV. DISCUSSION

In this work, we have investigated the photoacoustic-imaging-guided microbubble-mediated intravascular sonothrombolysis with a customized 10-Fr dual-lumen ultrasound catheter. With a compact design, the low-frequency, forward-firing stacked transducer delivered the acoustic energy directly at the clot surface, which showed promising lysis efficiency and the capability of flow restoration with low ultrasound input power. By comparing the clot dissolution rate under different conditions (US+MB, US-only, MB-only), the

microbubble-mediated sonothrombolysis was the most effective. Especially, different from the clot surface deduction with US-only treatment, the US+MB treatment showed great improvement in recanalization. To investigate the mechanism of the US+MB treatment, the passive cavitation detection under different conditions were conducted. The passive cavitation detection confirmed that the elevated inertial cavitation dose (about five times stronger) contributed to the improved lysis rate in the US+MB treatment over the US-only treatment, which was also consistent to the previous reports [16], [18]. A duty cycle similar with previous study was applied in this work, which was less than 5% and was confirmed to be safe without causing vessel damage or hemorrhage as observed by H&E histology [28].

Compared with our previously reported work that was focused on the therapeutic stacked transducer development, this work integrated PA imaging guidance for real-time thrombus detection in deep tissue. Moreover, taking advantage of the compact structure, an optical fiber was integrated to the catheter. With the laser locally delivered to the clot, II-PAT was achieved in deep tissue during the sonothrombolysis process. II-PAT was able to provide detailed information about the clot characteristics such as size, stiffness, and oxygenation, and was highly compatible with the sonothrombolysis procedure without any signal interference. Since the clots were immersed in highly oxygenated PBS, the treatment process may gradually Simprove the oxygen diffusion into the clots by loosening the clot structure. Unlike conventional ultrasound B-mode imaging, II-PAT can clearly differentiate the boundary between the catheter tip and the clot surface in deep tissue, which can provide the correct transducer position during the treatment [46]. With the internal light delivery, II-PAT can provide an imaging depth of ten centimeters. In addition to detecting morphological change in the clots during the treatment, II-PAT also provided functional information such as clot sO_2 and stiffness. With near-infrared laser pulses at two different wavelengths delivered internally, clot sO_2 was estimated up to 5 mm from the clot surface. The estimated sO_2 was closely related to the clot age, as hemoglobin in fresh clots is expected to have higher oxygenation levels. Additional wavelengths can be used for clot composition study, such as fibrin, RBCs, and platelets, providing an alternative for on-site pathology analysis during the treatment. Our previous study has also shown that there is a strong correlation between the PA signal frequency spectrum components and the stiffness of the clots [46]. Retracted clots with RBC-rich structure were associated with low-frequency PA signals, while less retracted clot structures with low RBC density had stronger high-frequency components due to the presence of relatively small RBC clutters. Though frequency-dependent attenuation becomes non-negligible in deep tissue imaging for PA signals, frequency changes were still observed before and after the treatment. For more accurate results, the PA frequency spectra can be compensated with tissue frequency-dependent attenuation. Reference PA spectra from clots with different stiffness and chemical compositions can also be acquired. Though the clots were immersed in PBS for this study, PAT should be able to differentiate the clot and the surrounding blood based on sO_2 and PA signal spectrum [46]

Although the PA-imaging guided sonothrombolysis system showed promising results, there are several limitations in this work. The sonothrombolysis experiments were carried out with PBS as the medium for convenient observation of mass reduction. In the future work, a flow system with blood as the medium will be used to mimic *in vivo* conditions. Besides, the treatment transducer had limited penetration depth due to the small aperture size, which

made it more difficult in catheter positioning during treatment. A multi-element treatment transducer with a better penetration depth can be a potential solution. For PAT, the current method using a linear transducer array did not show the details of the 3D clot structure. To better monitor the treatment process, a 2D transducer array can provide volumetric imaging.

V. CONCLUSIONS

In this work, we reported photoacoustic-imaging-guided intravascular sonothrombolysis *in-vitro*. With microbubbles as the contrast agents, the cavitation signals were significantly increased under ultrasound excitation, which contributed to the improved lysis rate. Furthermore, an optical fiber was assembled with the treatment catheter for local laser light delivery, and PAT was applied for monitoring the clot reduction and characterizing the clot properties in deep tissue during the treatment. By analyzing the oxygenation level and acoustic frequency spectrum from the clots, photoacoustic imaging provided detailed clot composition and structural information. Our results have demonstrated that photoacoustic-imaging-guided sonothrombolysis is highly promising for treating the deep-tissue blood clots.

ACKNOWLEDGMENT

This work was supported by NIH grants R01HL141967 and R21EB027304. The authors acknowledge the technical support from Dr. Paul Dayton's lab at the University of North Carolina at Chapel Hill. Authors also thank the prototype catheter support from SonoVascular, Inc.

REFERENCES

[1]. Agnelli G and Becattini C, "Acute pulmonary embolism," N. Engl. J. Med, vol. 363, (3), pp. 266–274, 2010. [PubMed: 20592294]

[2]. Di Nisio M, van Es N and Büller HR, "Deep vein thrombosis and pulmonary embolism," The Lancet, vol. 388, (10063), pp. 3060–3073, 2016.

[3]. White RH, "The epidemiology of venous thromboembolism," Circulation, vol. 107, (23_suppl_1), pp. I–8, 2003.

[4]. Silverstein MD et al. , "Trends in the incidence of deep vein thrombosis and pulmonary embolism: a 25-year population-based study," Arch. Intern. Med, vol. 158, (6), pp. 585–593, 1998. [PubMed: 9521222]

[5]. Albers GW et al. , "Intravenous tissue-type plasminogen activator for treatment of acute stroke: the Standard Treatment with Alteplase to Reverse Stroke (STARS) study," Jama, vol. 283, (9), pp. 1145–1150, 2000. [PubMed: 10703776]

[6]. Scarvelis D and Wells PS, "Diagnosis and treatment of deep-vein thrombosis," Cmaj, vol. 175, (9), pp. 1087–1092, 2006. [PubMed: 17060659]

[7]. Streiff MB et al. , "Guidance for the treatment of deep vein thrombosis and pulmonary embolism," J. Thromb. Thrombolysis, vol. 41, (1), pp. 32–67, 2016. [PubMed: 26780738]

[8]. Fleck D et al. , "Catheter-directed thrombolysis of deep vein thrombosis: literature review and practice considerations," Cardiovascular Diagnosis and Therapy, vol. 7, (Suppl 3), pp. S228, 2017. [PubMed: 29399526]

[9]. Miller DJ, Simpson JR and Silver B, "Safety of thrombolysis in acute ischemic stroke: a review of complications, risk factors, and newer technologies," The Neurohospitalist, vol. 1, (3), pp. 138–147, 2011. [PubMed: 23983849]

[10]. Smith SJ et al. , "Vacuum-assisted thrombectomy device (AngioVac) in the management of symptomatic iliocaval thrombosis," Journal of Vascular and Interventional Radiology, vol. 25, (3), pp. 425–430, 2014. [PubMed: 24581466]

[11]. Rosenschein U et al. , “Ultrasound imaging–guided noninvasive ultrasound thrombolysis: preclinical results,” Circulation, vol. 102, (2), pp. 238–245, 2000. [PubMed: 10889137]

[12]. Heldin C and Westermark B, “Mechanism of action and in vivo role of platelet-derived growth factor,” Physiol. Rev, 1999.

[13]. Maxwell AD et al. , “Noninvasive thrombolysis using pulsed ultrasound cavitation therapy–histotripsy,” Ultrasound Med. Biol, vol. 35, (12), pp. 1982–1994, 2009. [PubMed: 19854563]

[14]. Maxwell AD et al. , “Noninvasive thrombolysis using pulsed ultrasound cavitation therapy–histotripsy,” Ultrasound Med. Biol, vol. 35, (12), pp. 1982–1994, 2009. [PubMed: 19854563]

[15]. Kim J et al. , “Intravascular forward-looking ultrasound transducers for microbubble-mediated sonothrombolysis,” Scientific Reports, vol. 7, (1), pp. 1–10, 2017. [PubMed: 28127051]

[16]. Goel L et al. , “Examining the influence of low-dose tissue plasminogen activator on microbubble-mediated forward-viewing intravascular sonothrombolysis,” Ultrasound Med. Biol, vol. 46, (7), pp. 1698–1706, 2020. [PubMed: 32389332]

[17]. Goel L and Jiang X, “Advances in sonothrombolysis techniques using piezoelectric transducers,” Sensors, vol. 20, (5), pp. 1288, 2020. [PubMed: 32120902]

[18]. Kim J et al. , “A comparison of sonothrombolysis in aged clots between low-boiling-point phase-change nanodroplets and microbubbles of the same composition,” Ultrasound Med. Biol, vol. 46, (11), pp. 3059–3068, 2020. [PubMed: 32800631]

[19]. Tachibana K and Tachibana S, “Albumin microbubble echo-contrast material as an enhancer for ultrasound accelerated thrombolysis,” Circulation, vol. 92, (5), pp. 1148–1150, 1995. [PubMed: 7648659]

[20]. Hitchcock KE et al. , “Ultrasound-enhanced rt-PA thrombolysis in an ex vivo porcine carotid artery model,” Ultrasound Med. Biol, vol. 37, (8), pp. 1240–1251, 2011. [PubMed: 21723448]

[21]. Bader KB, Gruber MJ and Holland CK, “Shaken and stirred: mechanisms of ultrasound-enhanced thrombolysis,” Ultrasound Med. Biol, vol. 41, (1), pp. 187–196, 2015. [PubMed: 25438846]

[22]. Chaussy CG and Thüroff S, “High-intensity focused ultrasound for the treatment of prostate cancer: a review,” Journal of Endourology, vol. 31, (S1), pp. S–37, 2017.

[23]. Xu S et al. , “Dependence of pulsed focused ultrasound induced thrombolysis on duty cycle and cavitation bubble size distribution,” Ultrason. Sonochem, vol. 22, pp. 160–166, 2015. [PubMed: 25043556]

[24]. Zhang X et al. , “Histotripsy thrombolysis on retracted clots,” Ultrasound Med. Biol, vol. 42, (8), pp. 1903–1918, 2016. [PubMed: 27166017]

[25]. Rosenschein U et al. , “Ultrasound imaging–guided noninvasive ultrasound thrombolysis: preclinical results,” Circulation, vol. 102, (2), pp. 238–245, 2000. [PubMed: 10889137]

[26]. Wright C, Hynynen K and Goertz D, “In vitro and in vivo high intensity focused ultrasound thrombolysis,” Invest. Radiol, vol. 47, (4), pp. 217, 2012. [PubMed: 22373533]

[27]. Burgess A et al., “High-intensity focused ultrasound (HIFU) for dissolution of clots in a rabbit model of embolic stroke,” 2012.

[28]. Goel L et al. , “Safety evaluation of a forward-viewing intravascular transducer for sonothrombolysis: An in vitro and ex vivo study,” Ultrasound Med. Biol, vol. 47, (11), pp. 3231–3239, 2021. [PubMed: 34446331]

[29]. Rodger MA et al. , “Identifying unprovoked thromboembolism patients at low risk for recurrence who can discontinue anticoagulant therapy,” Cmaj, vol. 179, (5), pp. 417–426, 2008. [PubMed: 18725614]

[30]. Prandoni P et al. , “The risk of recurrent venous thromboembolism after discontinuing anticoagulation in patients with acute proximal deep vein thrombosis or pulmonary embolism. A prospective cohort study in 1,626 patients,” Haematologica, vol. 92, (2), pp. 199–205, 2007. [PubMed: 17296569]

[31]. Agnelli G et al. , “Extended oral anticoagulant therapy after a first episode of pulmonary embolism,” Ann. Intern. Med, vol. 139, (1), pp. 19–25, 2003. [PubMed: 12834314]

[32]. Mfoumou E et al. , “Time-dependent hardening of blood clots quantitatively measured in vivo with shear-wave ultrasound imaging in a rabbit model of venous thrombosis,” Thromb. Res, vol. 133, (2), pp. 265–271, 2014. [PubMed: 24315316]

[33]. Schmitt C, Henni AH and Cloutier G, “Characterization of blood clot viscoelasticity by dynamic ultrasound elastography and modeling of the rheological behavior,” J. Biomech, vol. 44, (4), pp. 622–629, 2011. [PubMed: 21122863]

[34]. Huang C, Wang S and Tsui P, “Detection of blood coagulation and clot formation using quantitative ultrasonic parameters,” Ultrasound Med. Biol, vol. 31, (11), pp. 1567–1573, 2005. [PubMed: 16286034]

[35]. Lensing AW et al. , “Detection of deep-vein thrombosis by real-time B-mode ultrasonography,” N. Engl. J. Med, vol. 320, (6), pp. 342–345, 1989. [PubMed: 2643771]

[36]. Mitchell DG, “Color Doppler imaging: principles, limitations, and artifacts.” Radiology, vol. 177, (1), pp. 1–10, 1990.

[37]. Huang C, Wang S and Tsui P, “In vitro study on assessment of blood coagulation and clot formation using doppler ultrasound,” Japanese Journal of Applied Physics, vol. 44, (12R), pp. 8727, 2005.

[38]. Szabo TL, Diagnostic Ultrasound Imaging. Amsterdam [u.a.]: Elsevier Academic Press, 2004.

[39]. Emelianov SY et al. , “Triplex ultrasound: elasticity imaging to age deep venous thrombosis,” Ultrasound Med. Biol, vol. 28, (6), pp. 757–767, 2002. [PubMed: 12113788]

[40]. Huang C, “High-frequency attenuation and backscatter measurements of rat blood between 30 and 60 MHz,” Physics in Medicine & Biology, vol. 55, (19), pp. 5801, 2010. [PubMed: 20844333]

[41]. Huang C et al. , “Determining the acoustic properties of the lens using a high-frequency ultrasonic needle transducer,” Ultrasound Med. Biol, vol. 33, (12), pp. 1971–1977, 2007. [PubMed: 17673358]

[42]. Davidson BL et al. , “Low accuracy of color Doppler ultrasound in the detection of proximal leg vein thrombosis in asymptomatic high-risk patients,” Ann. Intern. Med, vol. 117, (9), pp. 735–738, 1992. [PubMed: 1416575]

[43]. Palmeri ML and Nightingale KR, “What challenges must be overcome before ultrasound elasticity imaging is ready for the clinic?” Imaging in Medicine, vol. 3, (4), pp. 433, 2011. [PubMed: 22171226]

[44]. Liu X, Li N and Wen C, “Effect of pathological heterogeneity on shear wave elasticity imaging in the staging of deep venous thrombosis,” PLoS One, vol. 12, (6), pp. e0179103, 2017. [PubMed: 28614362]

[45]. Xia J, Yao J and Wang LV, “Photoacoustic tomography: principles and advances,” Electromagnetic Waves (Cambridge, Mass.), vol. 147, pp. 1, 2014. [PubMed: 25642127]

[46]. Tang Y et al. , “Deep thrombosis characterization using photoacoustic imaging with intravascular light delivery,” Biomedical Engineering Letters, vol. 12, (2), pp. 135–145, 2022. [PubMed: 35529341]

[47]. Li M et al. , “Internal-illumination photoacoustic computed tomography,” J. Biomed. Opt, vol. 23, (3), pp. 030506, 2018.

[48]. Ma Jianguo et al. , “A preliminary engineering design of intravascular dual-frequency transducers for contrast-enhanced acoustic angiography and molecular imaging,” IEEE Transactions on Ultrasonics, Ferroelectrics and Frequency Control, vol. 61, (5), pp. 870–880, 2014. [PubMed: 24801226]

[49]. Wu H et al. , “Dual-frequency intravascular sonothrombolysis: An in vitro study,” IEEE Trans. Ultrason. Ferroelectr. Freq. Control, vol. 68, (12), pp. 3599–3607, 2021. [PubMed: 34370663]

[50]. Henderson R and Schulmeister K, Laser Safety. 2003.

[51]. “ANSI Z136 Standards,” The Laser Institute, Aug. 11, 2017. https://www.lia.org/resources/laser-safety-information/laser-safety-standards/ansi-z136-standards (accessed Dec. 19, 2022).

[52]. Jeon S et al. , “Real-time delay-multiply-and-sum beamforming with coherence factor for in vivo clinical photoacoustic imaging of humans,” Photoacoustics, vol. 15, pp. 100136, 2019. [PubMed: 31467842]

[53]. Matrone G et al. , “The delay multiply and sum beamforming algorithm in ultrasound B-mode medical imaging,” IEEE Trans. Med. Imaging, vol. 34, (4), pp. 940–949, 2014. [PubMed: 25420256]

[54]. Deán-Ben XL and Razansky D, “On the link between the speckle free nature of optoacoustics and visibility of structures in limited-view tomography,” Photoacoustics, vol. 4, (4), pp. 133–140, 2016. [PubMed: 28066714]

[55]. Paltauf G et al. , “Experimental evaluation of reconstruction algorithms for limited view photoacoustic tomography with line detectors,” Inverse Problems, vol. 23, (6), pp. S81, 2007.

[56]. Goel L et al. , “Nanodroplet-mediated catheter-directed sonothrombolysis of retracted blood clots,” Microsystems & Nanoengineering, vol. 7, (1), pp. 1–7, 2021. [PubMed: 34567721]

[57]. Bamber JC, “Attenuation and absorption,” Physical Principles of Medical Ultrasonics, vol. 2, pp. 93–166, 1986.

[58]. Olsson SB et al. , “Enhancement of thrombolysis by ultrasound,” Ultrasound Med. Biol, vol. 20, (4), pp. 375–382, 1994. [PubMed: 8085294]

[59]. Suchkova V et al. , “Enhancement of fibrinolysis with 40-kHz ultrasound,” Circulation, vol. 98, (10), pp. 1030–1035, 1998. [PubMed: 9737524]

[60]. Kim J et al. , “An Analysis of Sonothrombolysis and Cavitation for Retracted and Unretracted Clots Using Microbubbles Versus Low-Boiling-Point Nanodroplets,” IEEE Trans. Ultrason. Ferroelectr. Freq. Control, vol. 69, (2), pp. 711–719, 2021.

[61]. Tranquart F et al. , “Clinical use of ultrasound tissue harmonic imaging,” Ultrasound Med. Biol, vol. 25, (6), pp. 889–894, 1999. [PubMed: 10461715]

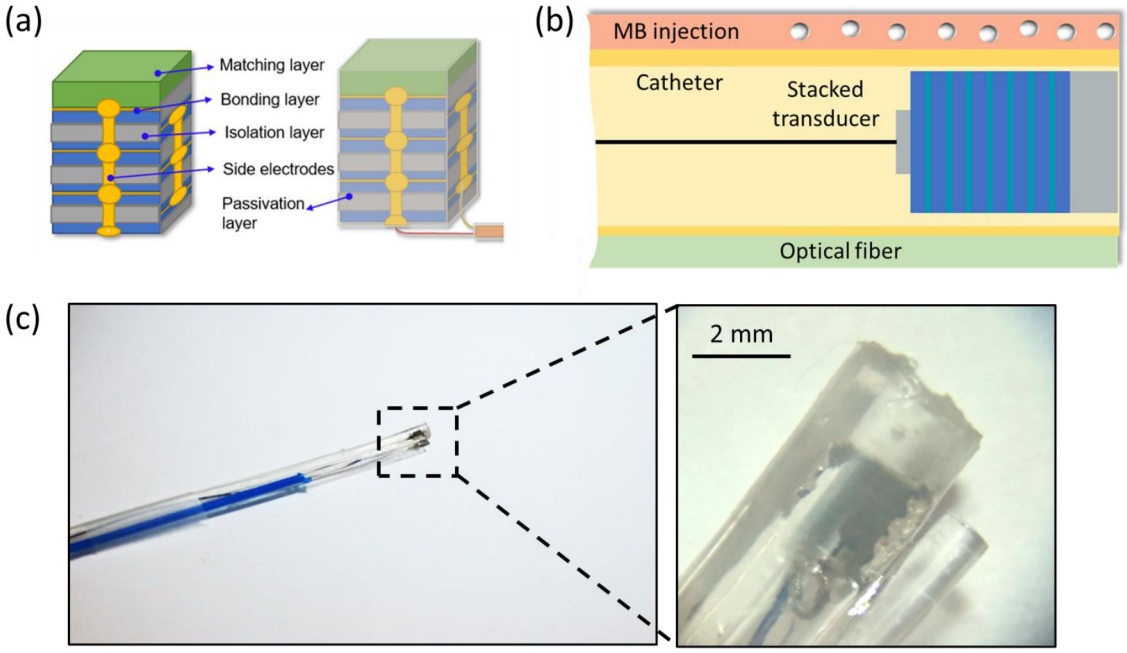

Fig. 1.

Schematic of the two-lumen catheter with the stacked transducer. (a) Structure of the stacked transducer. (b) Schematic of the relative position of the transducer, MB tube, and optical fiber. (c) Photograph of the fabricated stacked transducer integrated with the optical fiber.

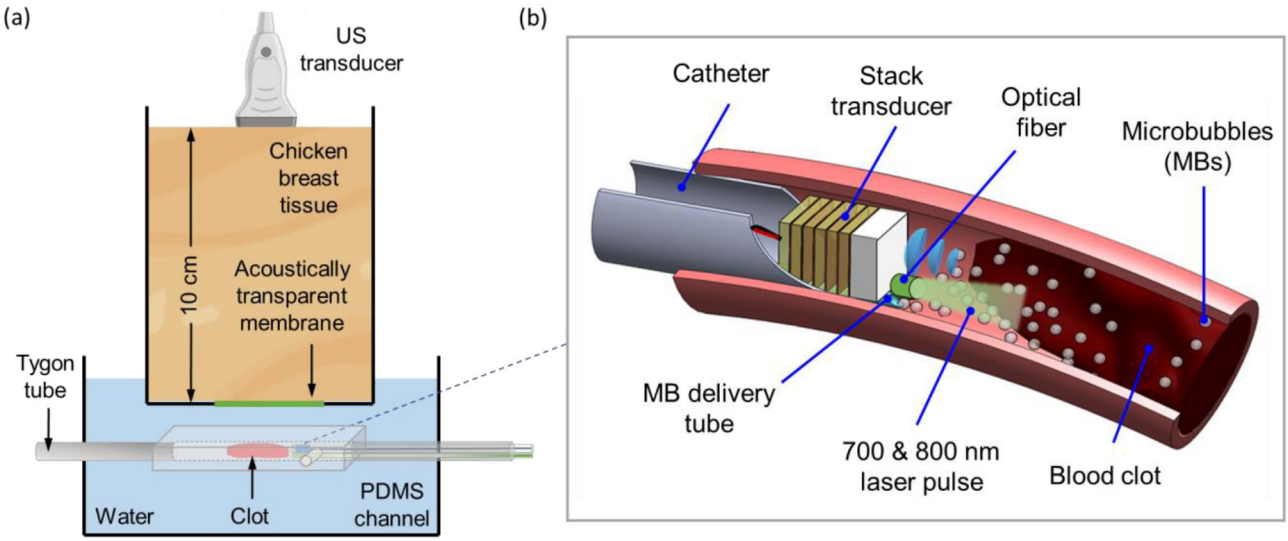

Fig. 2.

Schematic of the *in-vitro* sonothrombolysis with stacked transducer and internal-illumination photoacoustic imaging guidance. (a) Deep tissue clot detection with photoacoustic tomography. A Polydimethylsiloxane (PDMS) channel containing clot, catheter and optical fiber was immersed in water. A layer of ten-centimeter-thick chicken breast tissue was placed between the PDMS channel and the linear ultrasound transducer that was used for signal detection in photoacoustic imaging. (b) Interior design of the two-lumen catheter for the sonothrombolysis. The miniaturized stacked transducer was mounted in the main lumen with a side lumen for the microbubble (MB) delivery and laser light delivery.

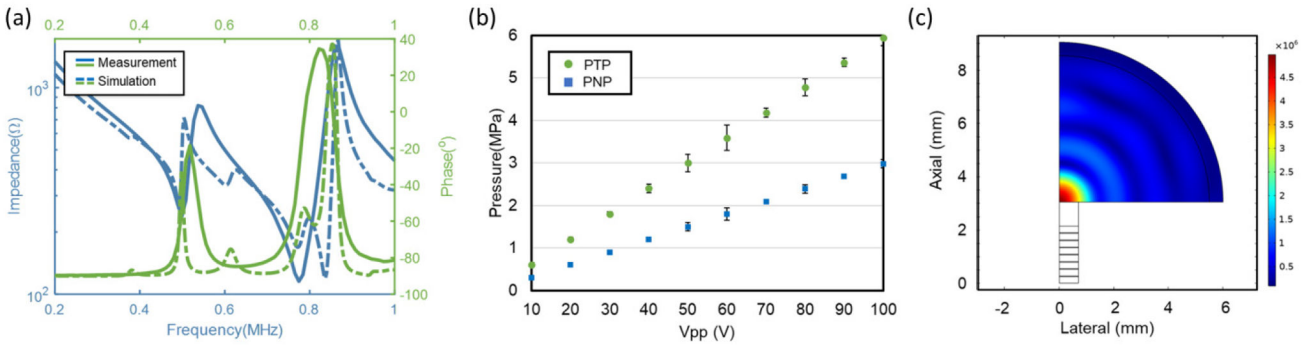

Fig. 3.

(a) Simulated and measured impedance curve for the stacked transducer from 0.2 MHz to 1.0 MHz. (b) Measured peak-to-peak (PTP) pressure and peak-negative pressure (PNP) for the stacked transducer with peak-to-peak input driving voltage (Vpp) from 10 V to 100 V (c) Simulated pressure output of the stacked transducer.

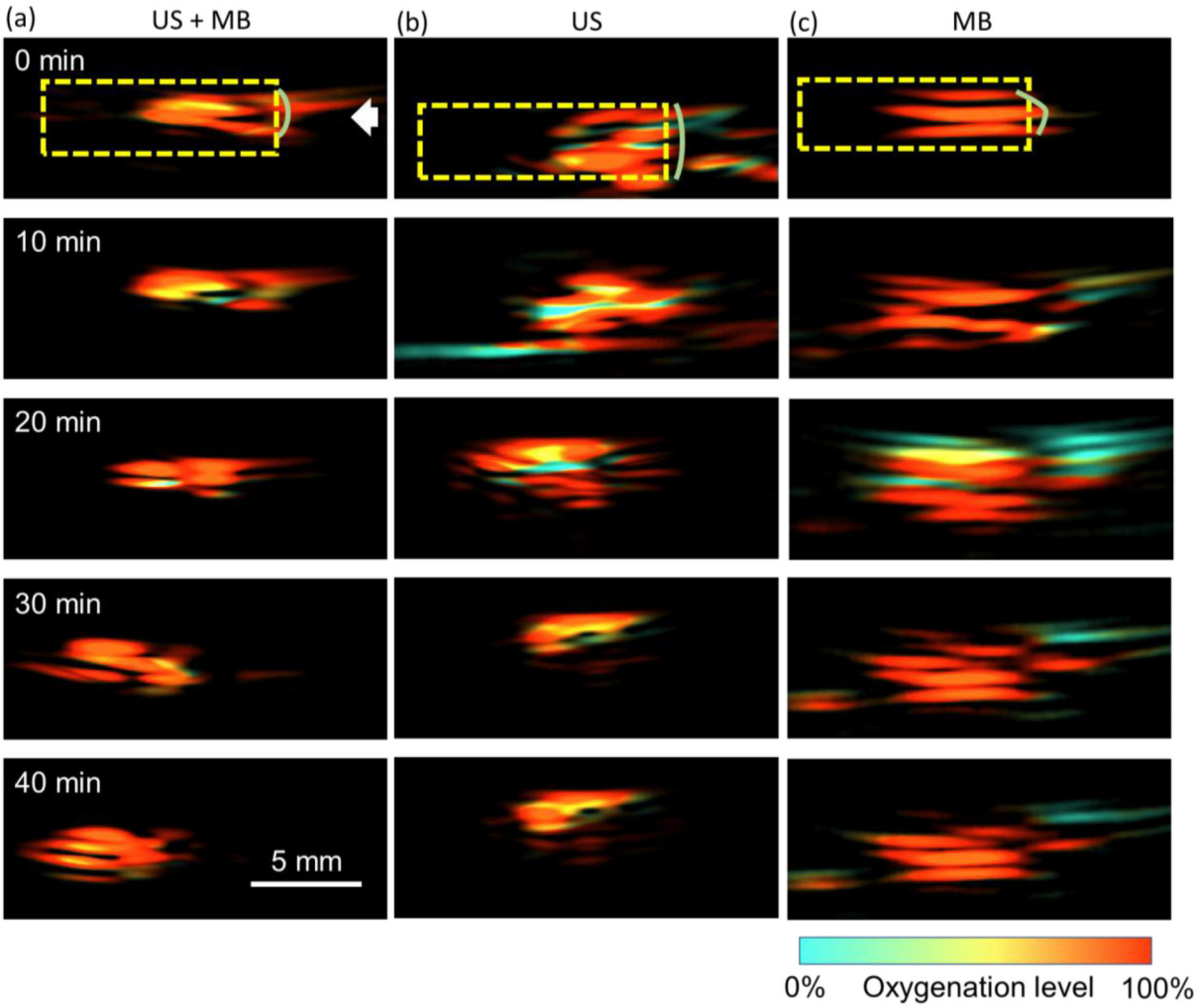

Fig. 4.

sO2 images of the blood clots beneath ten-centimeter chicken tissue, acquired every 10 minutes with three different treatment conditions: (a) Ultrasound treatment with infusion of microbubbles, (b) Ultrasound treatment only, (c) Microbubble infusion only. The original clot front end is marked by the solid green line and the original clot size is marked by the dashed yellow line. The white arrow indicates the direction of the catheter. The layered structures of the clot may be due to the streaking imaging artifacts as a result of the limited detection aperture of the imaging transducer array. The reverberation of the photoacoustic signals by the tube wall may also contribute to be layered image.

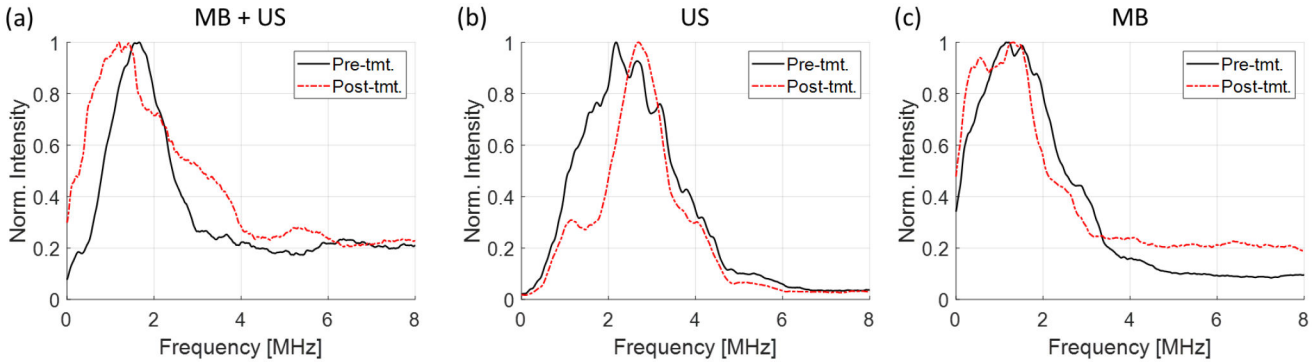

Fig. 5.

Acoustic frequency spectra of PA signals acquired at 800 nm before and after the treatment under three conditions: (a) US+MB, (b) US-only, and (c) MB-only. Pre-tmt, pre-treatment; Post-tmt, post-treatment. Fig. 6 Passive cavitation detection under the US+MB and US-only treatment conditions. Averaged frequency amplitude spectra of the test groups for (a) stable cavitation and (b) inertial cavitation (N = 7) (c) Calculated cavitation dose for the inertial cavitation and stable cavitation.

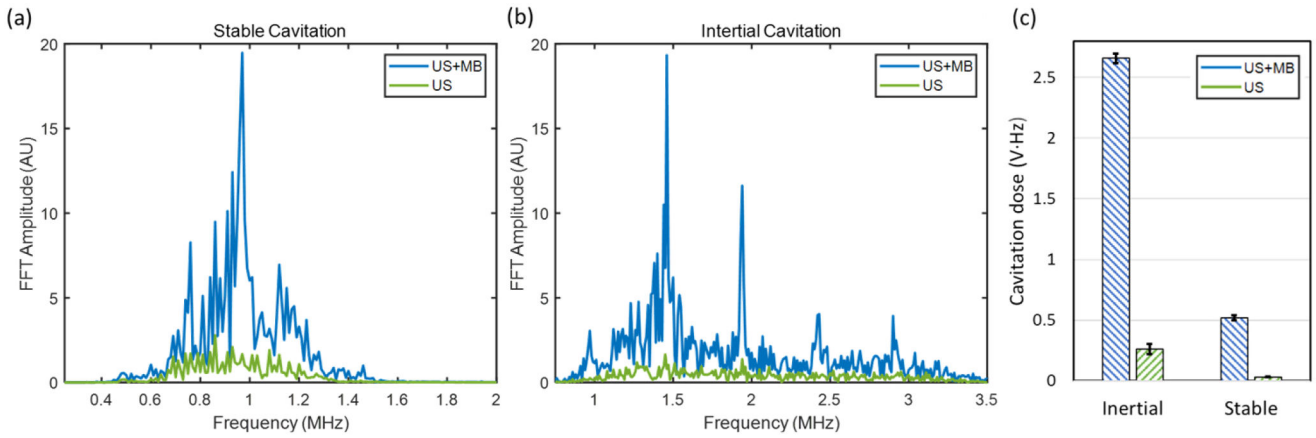

Fig. 6.

Clot size reduction and cross-sectional view after 40-min treatment under three treatment conditions: (a) Ultrasound treatment with microbubble infusion (b) Ultrasound treatment only (c) Microbubble infusion only.

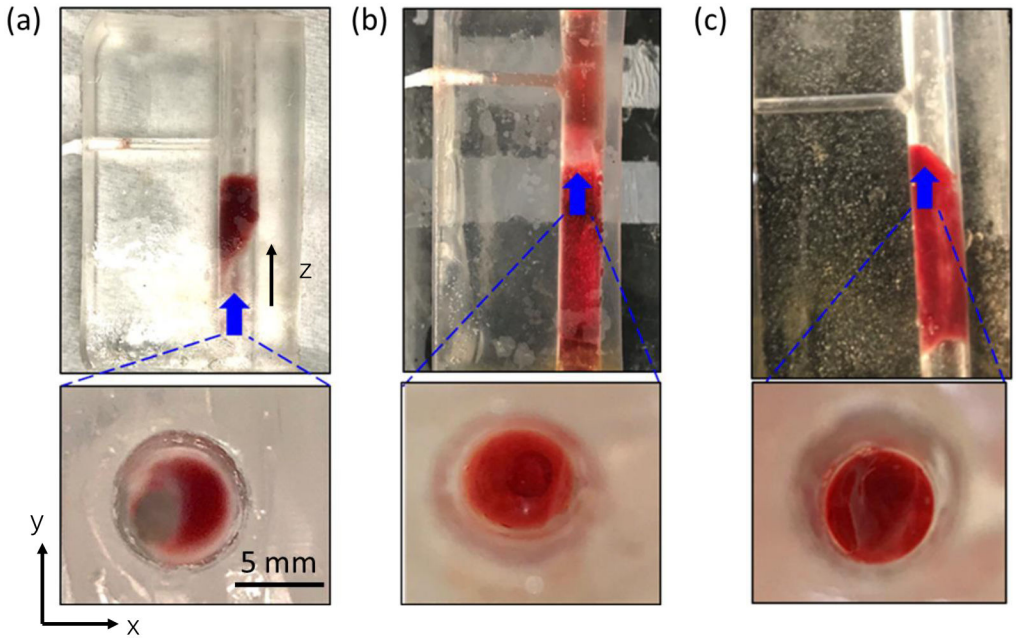

Fig. 7.

Clot size reduction and cross-sectional view after 40-min treatment under three treatment conditions: (a) Ultrasound treatment with microbubble infusion (b) Ultrasound treatment only (c) Microbubble infusion only.

TABLE I

Design parameters for the treatment transducer

	Material	Thickness	Velocity	Density	Acoustic Impedance
Active layer	PZT-5A	250 μm	4350 m/s	7750 kg/m^3	33.7 MRayl
Matching layer	$A1_2O_3$/epoxy	1.0 mm	2770 m/s	1300 kg/m^3	3.6 MRayl
Insulation layer	Al_2O_3/epoxy	50 μm	2770 m/s	1300 kg/m^3	3.6 MRayl
Passivation layer	Parylene C	13 μm	2200 m/s	1290 kg/m^3	2.8 MRayl
Bonding layer	E-solder 3022 (centrifuged)	25 μm	1850 m/s	3200 kg/m^3	5.9 MRayl